The Astrophysical Journal, 719:1470–1480, 2010 August 20 doi:10.1088/0004-637X/719/2/1470

DARK MATTER HALOS AND EVOLUTION OF BARS IN DISK GALAXIES: VARYING GAS FRACTION AND GAS SPATIAL RESOLUTION

Jorge Villa-Vargas[1], Isaac Shlosman[1], and Clayton Heller[2]
[1] Department of Physics and Astronomy, University of Kentucky, Lexington, KY 40506-0055, USA
[2] Department of Physics, Georgia Southern University, Statesboro, GA 30460, USA
Received 2010 April 24; accepted 2010 June 11; published 2010 July 30

ABSTRACT

We conduct numerical experiments by evolving gaseous/stellar disks embedded in live dark matter halos aiming at quantifying the effect of gas spatial resolution and gas content on the bar evolution. Three model sequences have been constructed using different resolutions, and the gas fraction has been varied along each sequence within the range of $f_g = 0\%$–50%, but keeping the disk and halo properties unchanged. We find that the spatial resolution becomes important with an increase in the gas content. For the higher resolution model sequences, we observe a bimodal behavior in the bar evolution with respect to the gas fraction, especially during the secular phase of this evolution. The switch from the gas-poor to gas-rich behavior is abrupt and depends on the resolution used, being reasonably confined to $f_g \sim 5\%$–12%. The diverging evolution has been observed in nearly all basic parameters characterizing bars, such as the bar strength, central mass concentration, bar vertical buckling amplitude, bar size, etc. We find that the presence of the gas component severely limits the bar growth and affects its pattern speed evolution. Gas-poor models display rapidly decelerating bars, while gas-rich models exhibit bars with constant or even slowly accelerating tumbling. We also find that the gas-rich models have bar corotation (CR) radii within the disk at all times, in contrast with gas-poor and purely stellar disks. In addition, the CR-to-bar size ratio is less than 2 for gas-rich models. Next, we have confirmed that the disk angular momentum within the CR remains unchanged in the gas-poor models, as long as the CR stays within the disk, but experiences a sharp drop before leveling off in the gas-rich models. Finally, we discuss a number of observed correlations between various parameters of simulated bars, such as between the bar sizes and the gas fractions, between the bar strength and the buckling amplitude, and between the bar strength and its size, etc.

Key words: galaxies: evolution – galaxies: halos – galaxies: kinematics and dynamics – galaxies: spiral – galaxies: structure – stars: kinematics and dynamics

1. INTRODUCTION

Many issues related to the formation and evolution of galactic bars remain unsettled (e.g., Villa-Vargas et al. 2009, hereafter Paper I). In Paper I, we have revisited the properties of barred disks embedded in the dark matter (DM) halos, with an emphasis on the angular momentum redistribution in *collisionless* systems. Here, we attempt to understand some effects of the gas component on the bar evolution. In a follow-up work, we investigate the effect of varying the halo parameters in the gaseous/stellar disk models.

Due to its viscous and dissipative nature, the gas can influence the stellar component in the disk, well beyond its observed mass fraction (e.g., Shlosman & Noguchi 1993; Friedli & Benz 1993; Heller & Shlosman 1994; Berentzen et al. 1998; Berentzen et al. 2007; Bournaud & Combes 2002; Curir et al. 2007). The gas dissipation, especially in the bar's presence, triggers the mass redistribution in the disk. A substantial fraction of barred orbits are self-intersecting, which while irrelevant for stars has a strong effect on the gas. The gas populating such orbits is short lived, resulting in shocks and loss of rotational support. Different viscosities in gas and stellar "fluid" lead to a delayed response to the gravitational torques and to an exchange of angular momentum between these components. The loss of angular momentum in the gas induces a flow down to the inner disk, forming a central mass concentration (CMC), and possibly forming and fueling the central supermassive black hole (SBH) via nested bars mechanism (e.g., Shlosman et al. 1989, 1990; Pfenniger & Norman 1990; Friedli & Martinet 1993; Knapen et al. 1995; Begelman & Shlosman 2009; Hopkins & Quataert 2010), and additional processes closer to the SBH (e.g., Shlosman 1999; Hopkins & Quataert 2010). The gas is capable of modifying the disk orbital structure (e.g., Berentzen et al. 1998). Moreover, the cold gas is inherently clumpy which effectively heats up the stellar "fluid" and populates the disk with an increased fraction of chaotic orbits, resulting in a decay of the bar strength (e.g., Shlosman & Noguchi 1993; Berentzen et al. 2007). The vertical buckling instability in the bar is progressively damped by the two-fluid gas–star interaction (e.g., Berentzen et al. 2007).

Formation and evolution of stellar bars is intricately related to the redistribution of angular momentum, J, in the disk-halo system. This means the presence of sources and sinks of angular momentum. Sellwood (1981) has shown that the former reside in the disk and the latter in the DM halo (see also Debattista & Sellwood 1998; Athanassoula 2002). Interactions of sources and sinks of J are dominated by resonances (Lynden-Bell & Kalnajs 1972; Athanassoula 2002; Martinez-Valpuesta et al. 2006; Paper I). Details of these resonance interactions are not fully understood and quantified. This is especially true in the presence of the gas component, as the above cited works are based on a purely collisionless modeling.

In this paper, we analyze the effect of the gaseous component on the evolution of galactic bars and take a numerical approach. In particular, we vary the gas content in the disk and advance models with various numerical resolution, but keep the stellar disk and DM halo parameters unchanged, using the standard model of Paper I. We are especially interested in how the gas presence and the associated numerical resolution affect the basic parameters of a stellar bar, as well as the angular momentum transfer process in a barred disk and in a disk-halo system. For this purpose, we perform a detailed comparison of models with gas to the standard collisionless model published in Paper I.

2. NUMERICS AND MODELING

We use the hybrid *N*-body and smooth particle hydrodynamics (SPH) FTM-4.4 code (e.g., Heller & Shlosman 1994; Heller et al. 2007; Romano-Diaz et al. 2009) to evolve the stellar and gaseous disks embedded in the DM halos. The gravitational forces are calculated using the FalcON routine (Dehnen 2002) which scales as O(N). The adopted units are the same as in Paper I: the units of mass and distance are taken as $10^{11}\,M_{\odot}$ and 10 kpc, respectively. This makes the unit of time equal to 4.7×10^7 yr, when $G = 1$, and the velocity unit 208 km s^{-1}. The gravitational softening is $\epsilon_{\rm grav} = 0.016$ for stars and DM particles. For the gas particles we use a dynamical softening. The gravitational softening is set to the smoothing length unless the smoothing length falls below the fixed limiting value $\epsilon_{\rm dyn}$. The models consist of a stellar disk with $N_* = 2 \times 10^5$, a gas disk with $N_{\rm gas} = 4 \times 10^4$, and DM halo with $N_{\rm DM} = 10^6$ collisionless particles. Models were evolved for about a Hubble time, $\Delta t = 270$ in the adopted units, which translates to 12.7 Gyr.

During the model evolution, we have routinely observed the formation of very compact accumulations of gas particles in the central disk region. In the models with a substantial gas component, we have observed the formation of secondary gaseous bars which decoupled from the large-scale bars and contracted subsequently to spatial scales where insufficient resolution resulted in flattened "blobs" a few softening lengths in radius, in agreement with simulations of Englmaier & Shlosman (2004). Besides the gradual capture of additional gas particles, the morphological structure of the blob has evolved very little and was beyond the resolution of our models. For the sake of shortening the computational time, we have replaced the gas particles trapped in the center by stellar ones. This operation was repeated whenever the central gas accumulation was substantially slowing down the overall evolution. We kept the softening of the individual particles when they were converted from one type to the other. We have run a large number of tests to verify that this action did not affect the evolution of the bar. This was achieved by running parallel models with and without the gas particle replacement.

2.1. Initial Conditions and Model Parameters

The initial conditions of the stellar and DM particles were created with the procedures described in Paper I, using the density profiles from Hernquist (1993). The mass volume density distribution in the disk is given in cylindrical coordinates by

$$\rho_{\rm d}(R, z) = \frac{M_{\rm d}}{4\pi h^2 z_0} \exp(-R/h)\,\mathrm{sech}^2\left(\frac{z}{z_0}\right), \qquad (1)$$

where $M_{\rm d}$ is the disk mass, h is a radial scale length, and z_0 is a vertical scale height. The density of the spherical halo is given by

$$\rho_{\rm h}(r) = \frac{M_{\rm h}}{2\pi^{3/2}} \frac{\alpha}{r_{\rm c}} \frac{\exp\left(-r^2/r_c^2\right)}{r^2 + \gamma^2}, \qquad (2)$$

where $M_{\rm h}$ is the mass of the halo, $r_{\rm c}$ is a Gaussian cutoff radius, and γ is the core radius. α is the normalization constant defined by

$$\alpha = \{1 - \sqrt{\pi} q \exp(q^2)[1 - \mathrm{erf}(q)]\}^{-1} \qquad (3)$$

with $q = \gamma/r_{\rm c}$. The particle velocities, dispersion velocities, and asymmetric drift corrections were calculated using moments of the collisionless Boltzmann equation. Since models thus constructed are not in exact virial equilibrium, the halo component was relaxed for $t \sim 40$ in the frozen disk potential.

Table 1
Parameters of the Standard Model

Halo		Disk	
Parameter	Value	Parameter	Value
$N_{\rm DM}$	10^6	N_*	2×10^5
$M_{\rm h}$	3.15	$M_{\rm d}$	0.63
$r_{\rm t}$	8.55	$R_{\rm t}$	1.71
γ	0.1425	h	0.285
$r_{\rm c}$	2.85	z_0	0.057
		Q_*	1.5

Notes. Q_* is the Toomre parameter for the stellar component fixed at $R = 2.4h$, where h is the thickness of the disk; $r_{\rm t}$ and $R_{\rm t}$ are numerical truncation radii in the halo and the disk. All values are given in dimensionless units, Section 2.

Table 2
Gas Fractions and Limiting Dynamical Softening in the Model Sequences

Model	$f_{\rm g}(\%)$	$\epsilon_{\rm grav}$
SD	0	...
SD_G2S1	2	0.016
SD_G4S1	4	0.016
SD_G8S1	8	0.016
SD_G15S1	15	0.016
SD_G30S1	30	0.016
SD_G50S1	50	0.016
SD_G2S2	2	0.050
SD_G4S2	4	0.050
SD_G8S2	8	0.050
SD_G15S2	15	0.050
SD_G30S2	30	0.050
SD_G50S2	50	0.050
SD_G2S3	2	0.10
SD_G4S3	4	0.10
SD_G8S3	8	0.10
SD_G15S3	15	0.10
SD_G30S3	30	0.10
SD_G50S3	50	0.10

Notes. All values are given in dimensionless units, Section 2. Columns: (1) model sequences; (2) gas fractions in %; (3) gravitational softening in the gas.

Because we are interested in quantifying the effect of the gas fraction and *gas* spatial resolution on the bar evolution, we use the pure stellar model SD from Paper I as our benchmark model (Table 1). A fixed fraction $f_{\rm g}$ of stellar disk particles at $t = 0$ were converted to identical mass gas particles and re-balanced using the central attraction forces from the total mass distribution. The gas is considered to be isothermal with $T_{\rm gas} = 10^4$ K and initially moves on circular orbits.

We have created a set of models covering a two-dimensional parameter space: by varying the gas mass fraction, $f_{\rm g}$, in the disk, and by changing the limiting value of the gravitational softening, $\epsilon_{\rm dyn}$, in the gas. The sum of stellar+gas mass was kept constant in the models. We used the values $f_{\rm g} = 0\%$, 2%, 4%, 8%, 15%, 30%, and 50%, and $\epsilon_{\rm grav} = 0.016$, 0.05, and 0.1. The softening used for the stellar and DM components is fixed at 0.016. Table 2 shows the combination of $f_{\rm g}$ and $\epsilon_{\rm grav}$ values used in each model.

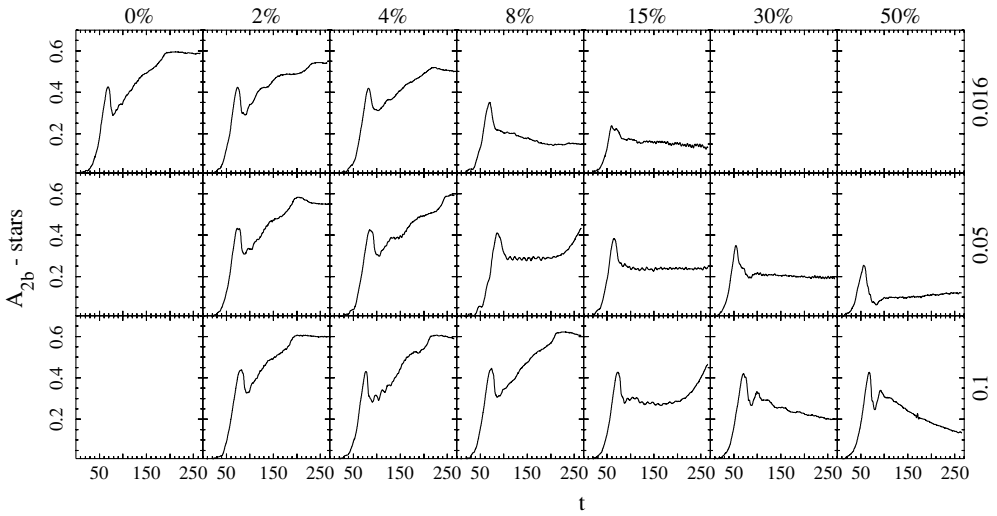

Figure 1. Time evolution of normalized bar amplitudes A_{2b}. Rows correspond to models of equal dynamical softening in the gas, ϵ_{grav}, indicated on the right. Columns correspond to models with equal gas fraction, f_g, indicated on the top. All the data have been smoothed with a lowpass Fourier filter.

3. RESULTS

Disks with a high content of gas tend to form dense clumps of gas which interact with the stellar component and raise the velocity dispersion in the disk. If this rise in the disk "temperature" is substantial, the bar instability may be lessened or completely suppressed (Shlosman & Noguchi, 1993). We have encountered this problem when evolving models with $f_g = 100\%$ which prevented us from completing these runs.

3.1. Bar Strength

The *stellar* bar strength has been quantified using the Fourier amplitude A_{2b} of the $m = 2$ mode normalized by the $m = 0$ mode (Paper I). It is obtained by integration over restricted cylindrical volumes where the bar is a dominant morphological feature, namely, over $R = 0.1-R_b$ range, where R_b is the bar size defined in Section 3.3 (see also Paper I). In Figure 1, we plot A_{2b} as a function of time t for various gas fractions, f_g, and gravitational softening in the gas, ϵ_{grav}. The initial stages in the evolution of A_{2b} are very similar in all models: an initial stage of an accelerated growth and a peak followed by a sudden drop. The duration of this dynamical stage varies from model to model, but is completed by $t \sim 100$.

The first peak in A_{2b} is followed by the vertical buckling instability in the bar leading to an abrupt weakening in the bar but not a complete dissolution (e.g., Martinez-Valpuesta & Shlosman 2004). We observe that the bar weakening is quite independent of f_g and ϵ_{grav}, as expected. For gas-poor models, the first peak of A_{2b} is independent of ϵ_{grav} and f_g. For gas-rich models, with $f_g \gtrsim 15\%$, the peak is lowered gradually for $\epsilon_{grav} \lesssim 0.05$, up to a factor of 0.4. Models with $\epsilon_{grav} = 0.1$ appear not to be affected at all by this trend.

The post-buckling evolution of the bars is much more affected by f_g and ϵ_{grav} and shows a bimodal behavior. Namely, in gas-poor models, the bar resumes its growth but at a more gradual pace as compared to the dynamical growth. In gas-rich models, the bar strength declines over the simulation (i.e., Hubble) time. This bimodal behavior was noted by Berentzen et al. (2007), but the current models show it more explicitly.

We shall refer to the first bar evolution phase, including the buckling, as the *dynamical* phase and to the subsequent evolution as the *secular* phase. The secular stage allows the separation of the secularly growing models from the secularly declining ones. In no models have the bars disappeared completely—at least a substantial oval distortion remained.

The borderline f_g between these two trends, growth and decline, depends on ϵ_{grav}. For $\epsilon_{grav} = 0.016$, it lies in the range of $f_g \sim 5\%$–7%. Larger ϵ_{grav} moves the borderline f_g toward more gas-rich models. Models SD_G8S2 and SD_G15S3 lie close to this borderline, $f_g \sim 8\%$–10% for $\epsilon_{grav} = 0.05$ and $f_g \sim 10\%$–12% for $\epsilon_{grav} = 0.1$ and show a very singular evolution—after the sudden drop $A_{2b} \sim$ const. for about $\Delta t \sim 100$, and a second period of bar growth begins. This is a surprisingly mixed behavior showing the prolonged constancy in A_{2b} of the gas-rich models and the secular bar growth of the gas-poor ones.

Model SD_G50S2 has a peculiar evolution in the dynamical stage that deserves special attention. Even though this is a gas-rich model, the bar resumes its secular growth after the buckling. The rate of growth is much more moderate than that in the other models but is clearly noticeable.

3.2. Pattern Speed

The evolution of the pattern speed Ω_b is shown in Figure 2. It remains about constant during the dynamical phase of the bar evolution, slightly rising in the gas-rich models. The bimodality of gas-poor and gas-rich models shows up in the secular evolution where Ω_b drops in the former and stays constant or rises in the latter disks. In the secular phase, Ω_b nearly always anti-correlates with A_{2b}. A sustained drop in Ω_b corresponds to a rise in A_{2b}. Thus, in the gas-poor models, the bar tumbling slows down, while in the gas-rich models it stays nearly constant.

Figure 2 provides a hint to what one can expect for the evolution of the angular momentum in the disk-halo system, although in no way does this figure account for *all* the angular momentum in the disk, and even in the bar region it represents only the tumbling of the bar. The gas-poor disks lose their tumbling angular momentum efficiently, while gas-rich ones nearly conserve it or even speed up their tumbling during the secular phase.

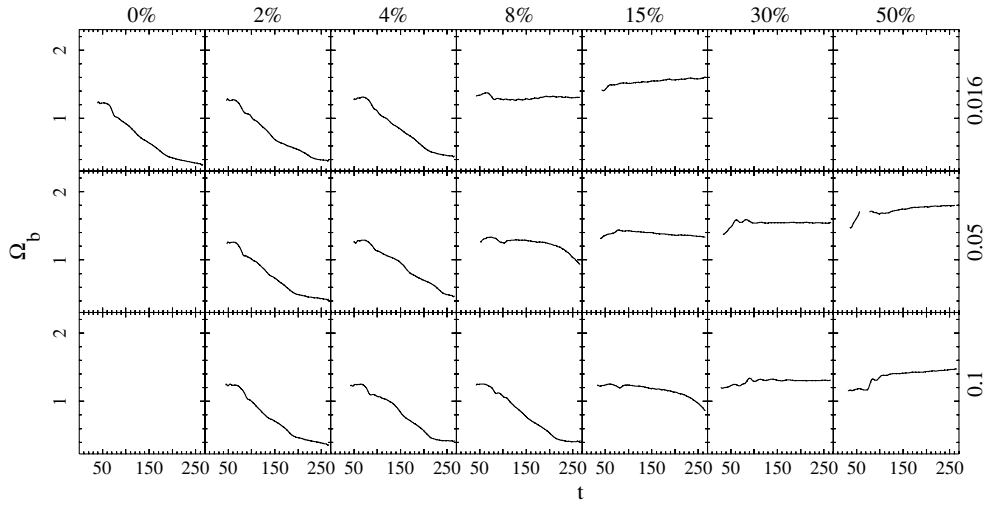

Figure 2. Time evolution of the bar pattern speed Ω_b. The distribution of models in rows and columns is that of Figure 1. Model SD_G50S2 curve has a gap around the time of the buckling. The bar weakens abruptly and its figure becomes distorted which makes it difficult to determine the pattern speed. Note that for the gas-rich disks, the pattern speed is a non-decreasing function of t. The gas fractions and spatial resolution are indicated at the top and on the right, respectively.

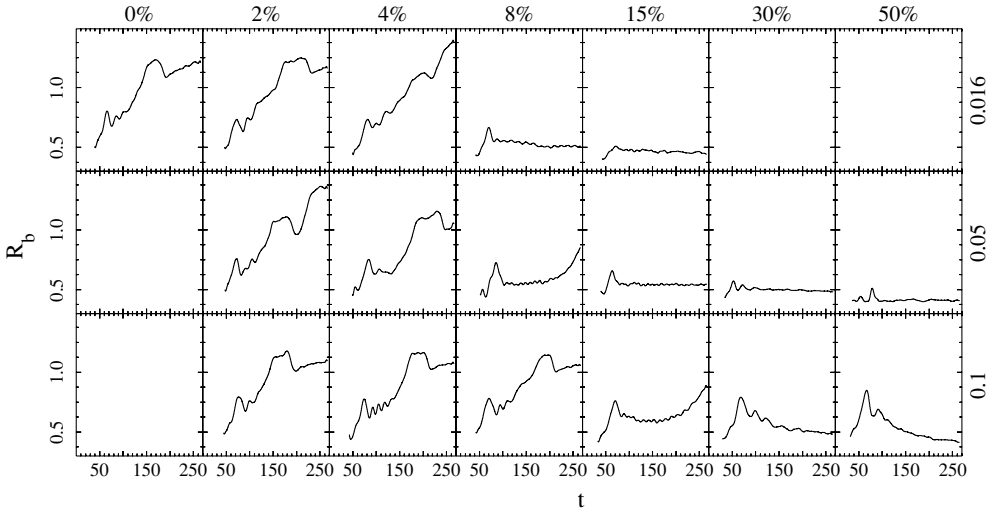

Figure 3. Time evolution of the bar semimajor-axis length R_b. The distribution of models in rows and columns is as in Figure 1. The bar sizes include the *ansae* (see the text). Note that bars are not growing in the secular phase in the gas-rich disks (see also SN93), and this is more pronounced in high resolution simulations. Gas fractions and resolution are indicated at the top and on the right, respectively.

3.3. Bar Length

The length of the bar semimajor axis, R_b, has been taken as the radius where the bar equatorial ellipticity drops by 15% off its peak (Paper I). This method has been tested in comparison with an alternative method based on the last stable orbit supporting the bar (Martinez-Valpuesta et al. 2006). It is the most reliable when applied after the first maximum of the bar strength. The ellipticity of the bar at different radii is obtained by fitting ellipses to the isodensity contours in the face-on disk. As in the collisionless models, the bar length exhibits the initial period of an accelerated growth and reaches a maximum which always coincides (in time) with the maximum in A_{2b} (Figure 3). This symbolizes the period of a dynamic growth of the bar, or growth related to the bar instability itself. Similarly to the pure stellar model, there is a subsequent drop in R_b as a result of the vertical buckling (Section 3.4). During the secular phase, the bar length exhibits a more complicated behavior than in the collisionless models. Most importantly, it grows in gas-poor models while it stagnates or even shortens in the gas-rich disks.

In the late stages of secular evolution, the gas-poor models show a sudden decrease in the bar size which has no immediate correspondence to A_{2b} evolution. Rather generally, the evolution of R_b does not go in tandem with changes in A_{2b}. As an example, in model SD_G4S1 after $t \sim 220$, R_b continues its growth while A_{2b} growth saturates. This behavior is caused by the formation, growth, and detachment of the *ansae*,[3] as discussed in Paper I. In the following, we shall show that R_b correlates with other properties of the bar-disk system.

The bar corotation (CR) radius R_{cr} has been computed using linear approximation. R_{cr} grows or shrinks as a consequence of the variation of the bar tumbling speed, Ω_b. It grows substantially in the SD and gas-poor models, while it stays constant or even drops slightly in the gas-rich models. Its initial value among all models is the same. As in Paper I, we follow the ratios of R_{cr} to that of the disk R_d (Figure 4) and bar R_b sizes.

[3] The ansae (i.e., handles) are typically found in early-type disk galaxies (Figure 11 in Martinez-Valpuesta et al. 2006; see also Martinez-Valpuesta et al. 2007), e.g., NGC 4262, NGC 2859, and NGC 2950 (Sandage 1961), NGC 4151 (Mundell & Shone 1999), and ESO 509-98 (Buta et al. 1998).

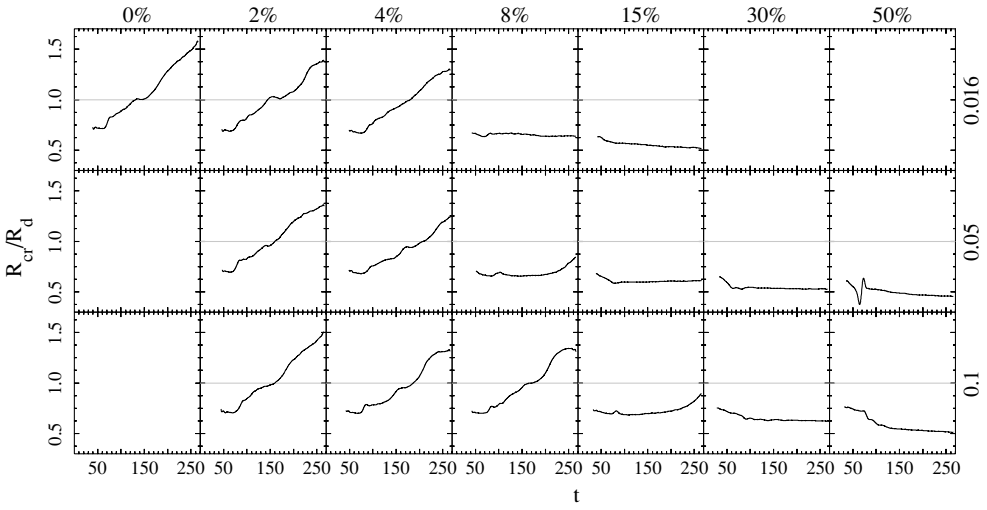

Figure 4. Time evolution of the ratio $R_{\rm cr}/R_{\rm d}$. The horizontal line has been added to help identify the time $R_{\rm cr}$ crosses the disk border. The distribution of models in rows and columns is as in Figure 1. Note that for the gas-rich disks the CR is always inside the disk, especially for higher resolution disks. Gas fractions and resolution are indicated at the top and on the right, respectively.

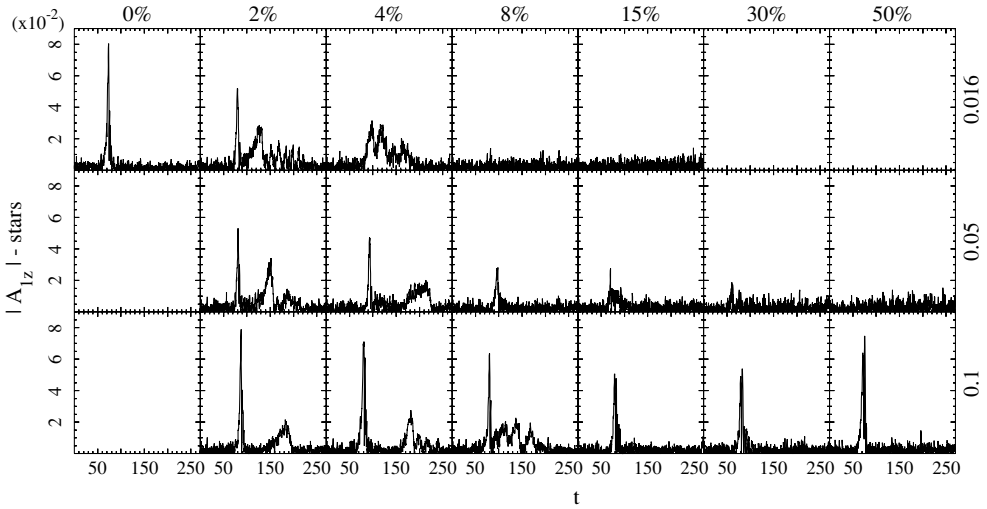

Figure 5. Evolution of the bar vertical asymmetry measured by the Fourier coefficient $|A_{1,z}|$ of the $m = 1$ mode in the rz-plane corotating with the bar major axis. No filtering was applied to this data. The distribution of models in rows and columns is as in Figure 1. Note that the first buckling amplitude decreases with $f_{\rm g}$, but the sequence $\epsilon_{\rm grav} = 0.1$ exhibits a somewhat more complicated behavior. In addition, $|A_{1,z}|$ correlates with $\epsilon_{\rm grav}$. Gas fractions and resolution are indicated at the top and on the right, respectively.

Both $R_{\rm d}$ and $R_{\rm b}$ have been defined in Paper I. Clearly, when $R_{\rm cr}/R_{\rm d} \sim 1$, its growth experiences a temporary slowdown and then resumes, rising to larger values. This effect is the result of the combination of a temporary slowdown of the outward radial movement of $R_{\rm cr}$ and a temporary expansion of the disk radial border which results from the drag on some of the disk material trapped at the CR resonance. As in the pure stellar models, the growth of the bar strength is sensitive to the moment at which $R_{\rm cr}$ crosses the edge of the disk, seen as a temporary period of slower growth of A_{2b}. Note that $R_{\rm cr}/R_{\rm d}$ is always less than unity in the gas-rich models and it seems that for a fixed $f_{\rm g}$ the CR-to-disk size ratio is damped stronger for small $\epsilon_{\rm grav}$, i.e., for higher numerical resolution.

The ratio $R_{\rm cr}/R_{\rm b}$ shows a pronounced dip during the initial growth of the bar. This is followed by an equally abrupt rise due to the bar shortening that results from the vertical buckling instability. After these variations, both $R_{\rm b}$ and $R_{\rm cr}$ grow in tandem, and $R_{\rm cr}/R_{\rm b} \sim 1.5 - 2 \pm 0.15$ in most of the models. Exceptions are model SD_G4S2 which has a rise and drop resulting from a temporary stall of $R_{\rm b}$, and models SD_G30S3 and SD_G50S3 where $R_{\rm cr} \sim$ const. while the bar shrinks. Finally, a pronounced rise above $R_{\rm cr}/R_{\rm b}= 2$ occurs in models due to detachment of the ansae (Paper I). This rise is absent in models in which no ansae are formed or which form too late in the run and do not have time to detach from the bar, as in SD_G15S3. We find that the ansae do not form in models with more than ∼10% of the gas. We note that the bar size evolution given in Figure 3 includes the ansae. However, in Section 4, we find it advantageous to exclude the ansae when discussing some correlations.

3.4. Vertical Buckling

The vertical buckling observed in many numerical bars is an event that in some cases can reshape the phase-space density of the disk. As we found in Paper I, when the disk is heated vigorously by the buckling instability, the secular growth of the bar can be seriously diminished or completely halted. We have measured the vertical asymmetry of the stellar disk with the index $A_{1,z}$, computed as described in Paper I. The evolution of $A_{1,z}$ is shown in Figure 5. Most of the models have at least one

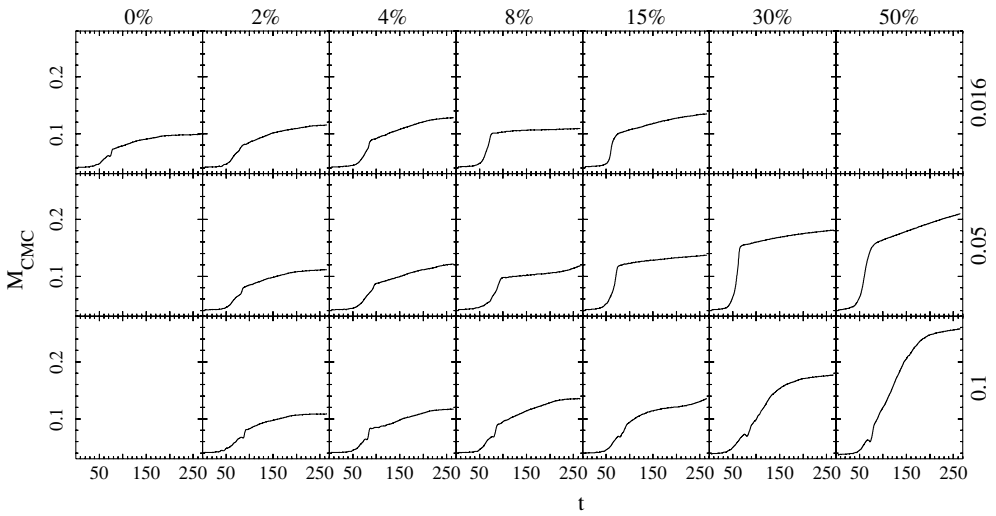

Figure 6. Time evolution of the central mass concentration (CMC): the total mass contained inside a sphere of radius 0.1 at the center of mass of the stellar disk. The stellar, gaseous, and DM components are included in the mass count. All the data have been smoothed with a high frequency Fourier filter. Gas fractions and resolution are indicated at the top and on the right, respectively.

clear peak between $t = 50$ and 100, and this peak coincides in time with the drop in A_{2b}. Exceptions are models SD_G15S1 and SD_G50S2, which have no clear peak above the noise level. Some models have secondary and even higher order peaks or prolonged periods where $A_{1,z}$ is clearly above the noise level, as found by Martinez-Valpuesta et al. (2006).

Clearly, the height of the first peak varies with the gas content of the disk. In the sequences with $\epsilon_{grav} = 0.016$ and 0.05, the peak becomes gradually lower in models with higher f_g. This result is in good agreement with Berentzen et al. (2007). The big surprise is in the sequence with $\epsilon_{grav} = 0.1$, where the value of the peak drops as f_g increases from 0% to 8%, and then rises in models with $f_g = 30\%$ and 50%. This is discussed further in Section 4.

The signature of the vertical buckling can be observed in the behavior of Ω_b. As the bar strengthens, it brakes against the outer disk and against the DM halo, at later time, and Ω_b declines. At the time of buckling, the bar weakens abruptly and Ω_b experiences a break—its slope changes and becomes much smaller.

3.5. Central Mass Concentration

One of the differences that arise between pure stellar models of galactic bars and models including a gas component is the formation of a CMC. The central densities, both stellar and DM, have notably increased even in pure stellar models as a response to the asymmetric potential of the bar and the vertical buckling (Paper I; Dubinski et al. 2009). However, this effect is by far more intense in models with gas. The growth of CMC is boosted by the bar which channels the gas toward the central kpc. This leads to a CMC composed mainly of gas, and, in smaller proportion, stellar, and DM particles. In all our models, the CMC has resided inside a radius smaller than 0.1.

To follow the growth of the CMC, we have measured the mass M_{CMC} contained within a sphere of radius 0.1 placed at the center of mass of the disk. Contributions from all three components have been included (Figure 6).

Model SD_G2S1 serves as a benchmark of evolution in the gas-poor models. With the formation of the stellar bar, a massive accumulation of gas appears at the center, with an elongated shape of $\sim 0.1 \times 0.04$, in the disk plane. This CMC is approximately aligned with the major axis of the (gas) bar. It rapidly captures the gas fed by the bar and simultaneously contracts into a small, more axisymmetric and somewhat flattened circular "blob" with $\Delta R \sim 0.04$ and $\Delta z \sim 0.01$. These characteristic sizes are determined largely by ϵ_{grav}. The accelerated M_{CMC} rise seen in Figure 6 encompasses the exponential bar growth phase, up to the time of buckling (or the time when A_{2b} drops in models with no buckling). Typically, about 50% of the gas mass is captured by the CMC during this stage.

During the secular phase of the bar evolution, the CMC captures the gas at a much slower pace. This is mostly the gas which remains outside R_b and even R_{cr} at the onset of the secular phase. The slowing down of the CMC growth results from a combination of two factors. First, the availability of the disk gas has been severely reduced by the violent initial inflow, and second, the bar strength has been diminished by the buckling. As a consequence, the gas-poor models have been left with very little gas in the disk after the initial inflow, although they show a healthy secular bar growth, whereas gas-rich models have gas left, but their bars are weak and do not grow, so no fresh gas crosses R_{cr} which stagnates as well.

Three models exhibit a somewhat different evolution for M_{CMC}. Instead of a short period of very accelerated growth, the CMC grows at a somewhat slower rate but over an extended period of time. These are models SD_G15S3, SD_G30S3, and SD_G50S3, which are all gas rich and have the lowest resolution. In these models, the gas content of the bar has formed without a visibly prominent CMC. Instead of a rapid influx to the center, the gas in the bar contracts rather slowly, gradually increasing its density at the center. The process saturates when the gas is completely contained within the central $R \sim 0.1$.

Models SD_G8S2 and SD_G15S3 show a rate of M_{CMC} growth that increases with time at the end of the run. This behavior is related to the late period of accelerated bar growth.

3.6. Angular Momentum

Angular momentum evolution in the disk has been followed within a number of characteristic radii, namely, the CR ($J_{d,in}$) and the disk radius, J_d (which contains 98% of the disk mass by definition). The latter exhibits a clear evolutionary sequence

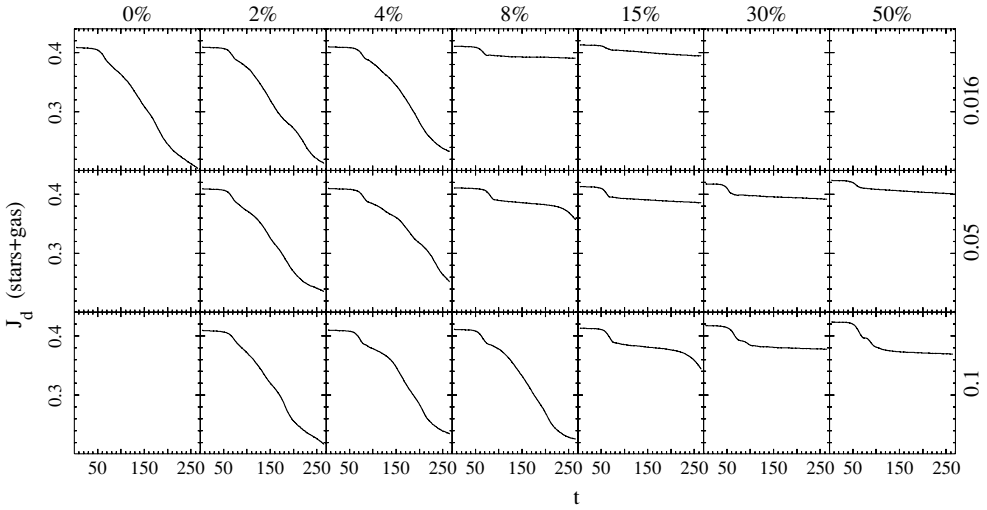

Figure 7. Time evolution of disk total angular momentum, $J_{\rm d}$. Gas fractions and resolution are indicated at the top and on the right, respectively.

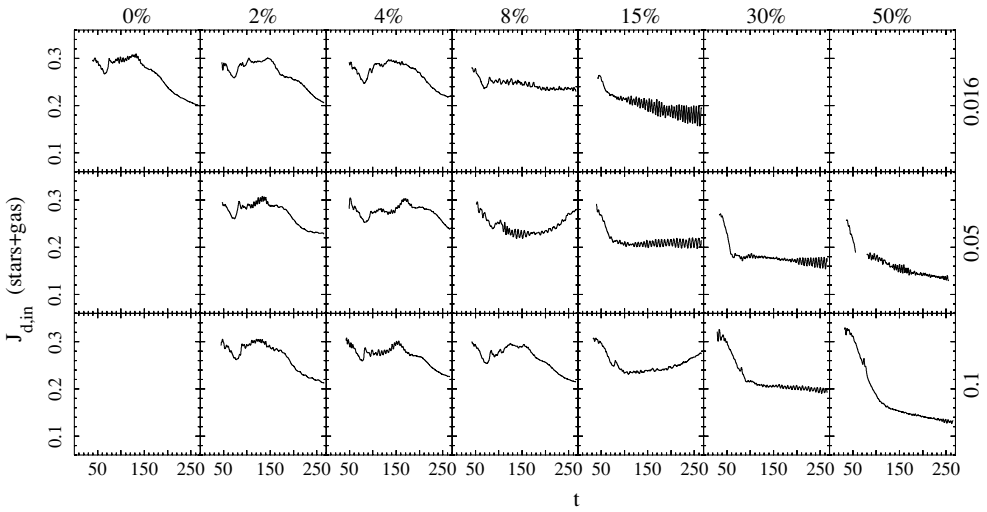

Figure 8. Time evolution of disk angular momentum inside the bar CR, $J_{\rm d,in}$. Note that $J_{\rm d,in} \approx$ const. in time as long as $R_{\rm cr}$ remains inside the disk, as can be seen from Figure 4. Gas fractions and resolution are indicated at the top and on the right, respectively.

as a function of $f_{\rm g}$ (e.g., Figure 7). Both the amount of J lost by the disk over dynamical and secular evolution decreases monotonically from pure stellar disks to progressively more gas-rich ones. In a way, this is a reflection of weaker bars along $f_{\rm g}$. Even more interesting is the evolution of $J_{\rm d,in}$ (Figure 8). After the initial adjustment, the disk within the CR is losing its angular momentum. The loss is not dramatic, ∼10%–20%, and somewhat increases with $f_{\rm g}$. This decline in $J_{\rm d,in}$ continues until the vertical buckling sets in. For low $f_{\rm g}$ disks, the buckling is associated with a nearly sudden increase in $J_{\rm d,in}$ which restores the pre-buckling value followed by a subsequent gradual decline. Gas-rich disks show no sudden increase in $J_{\rm d,in}$ but rather a slow decline.

$J_{\rm d,in}$ stays quite flat until $t \sim 150$, a long time after the buckling, as can bee seen from Figure 8 (with the exception of a small initial decline and increase, as mentioned above). Interestingly, this time corresponds to $R_{\rm cr}/R_{\rm d} < 1$ in the gas-poor models (Figure 4). Crossing the $R_{\rm cr}/R_{\rm d} = 1$ border affects the bar growth (Figure 3), which saturates immediately. It also is reflected in the evolution of $R_{\rm cr}/R_{\rm b}$ which increases abruptly thereafter. Clearly, the bar growth ceases at some point when the $R_{\rm cr}$ exceeds $R_{\rm d}$ and the bar cannot capture additional orbits and be fed by the angular momentum from these orbits. This situation is similar to that analyzed in Paper I (Section 3.6), where the angular momentum of the disk inside $R_{\rm cr}$ stays about constant as long as $R_{\rm cr}$ remains within the disk. Our present models can be directly compared to the standard model of Paper I. We return to this point in Section 4.

The loss of the angular momentum, $J_{\rm d,out}$, with $f_{\rm g}$ by the outer disk appears to be much more severe than $J_{\rm d,in}$. But one should remember that the outer disk, i.e., outside the CR, accounts for less mass. Before the buckling, $J_{\rm d,out}$ behaves similarly to $J_{\rm d,in}$, but differently at the later times. The trend here is that $J_{\rm d,out}$ declines steeply with time for gas-poor disks after the buckling period. It stays nearly constant with time for the gas-rich models.

Models with different $\epsilon_{\rm grav}$ show a behavior consistent with our understanding. There is a slight increase in the J transfer during dynamical and secular stages of the bar evolution. Much less difference is observed in the evolution of $J_{\rm d,in}$ and $J_{\rm d,out}$ in this case.

4. DISCUSSION: TESTING NEW CORRELATIONS

We have studied the effects of gas fraction, $f_{\rm g}$, and spatial resolution, $\epsilon_{\rm grav}$, on some aspects of bar evolution in galactic

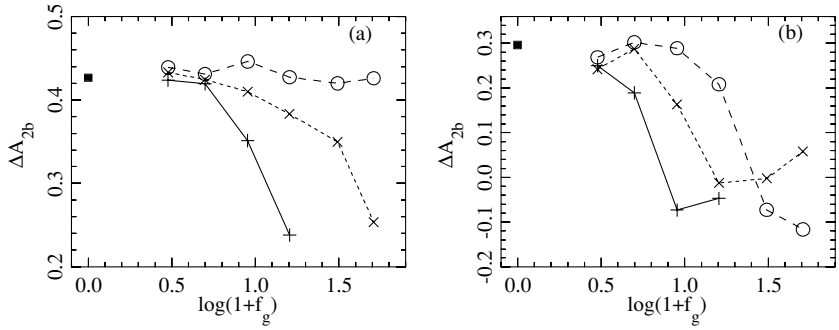

Figure 9. Bar strengthening during (*a*) dynamical and (*b*) secular phases of its evolution as a function of the gas fraction, f_g, for different spatial resolution in the gas, ϵ_{grav}, namely $\epsilon_{grav} = 0.016$ (crosses, solid lane), 0.05 (×, short dashed lane), and 0.1 (circles, long dashed lane). The filled square represents the SD model (Paper I) with no gas. The model SD_G8S1 has been omitted (see the text).

disks embedded in DM halos. Specifically, we aimed at understanding their effect on the basic parameters characterizing stellar bars, e.g., bar size, CR radius, strength, etc. We have also followed the angular momentum redistribution in the disk-halo systems as a function of f_g and ϵ_{grav}. The SD pure stellar model (Paper I) has been used as a template—the disk and halo parameters in current models have been fixed at those of the SD. As before, the bar evolution has been separated into two main phases—the dynamical phase, which represents the bar instability itself de facto, and the secular phase. These phases are separated by the vertical buckling instability in the bar. We investigate a number of new correlations which are corollaries to evolution discussed in Section 3. In the follow-up work (J. Villa-Vargas et al. 2010, in preparation), we analyze the angular momentum transfer and bar evolution as a function of disk gas fraction and by varying the basic parameters of the DM halo.

Overall, there appears to be a substantial difference in the evolution of the gas-poor and gas-rich models as has been shown in the previous section. This is discussed below in more detail. The boundary between the gas-poor and gas-rich models depends on the spatial resolution for the gas component—it lies around 5%–7% for $\epsilon_{grav} = 0.016$ and shifts to ∼10%–12% for $\epsilon_{grav} = 0.1$. The loss of spatial resolution, in a way, changes the nature of the gas component—it becomes less dissipative. We define the bar strengthening during its dynamical phase as $\Delta A_{2b} \equiv A_{2b}(t = t_{peak}) - A_{2b}(t = 0)$, where t_{peak} is the time when the bar has reached its maximal amplitude prior to the onset of buckling; the second term $A_{2b}(t = 0) = 0$. Similarly, the bar growth during the secular phase is defined as $\Delta A_{2b} \equiv A_{2b}(t = 270) - A_{2b}(t = t_{min})$, where t_{min} is the time of the minimal bar amplitude immediately following the buckling.

In the *dynamical* stage of the bar evolution, the largest differences have been observed in the gas-rich models, where ΔA_{2b} drops dramatically with f_g for $\epsilon_{grav} = 0.016$ and 0.05, while it exhibits no dependence on f_g for $\epsilon_{grav} = 0.1$ (Figures 1 and 9(a)). In the gas-poor models, the maximal bar amplitude achieved in the dynamical phase is nearly independent of the gas fraction, nor does it depend on the spatial resolution used in the modeling of the gas component (Figures 1 and 9(a)). Figure 9(a) supports the Berentzen et al. (1998, 2007) analysis that the increasing presence of the gas component makes the bar instability milder. In the *secular* stage, this sharp decrease in ΔA_{2b} with f_g persists, including the lowest resolution sequence as well. The bar growth is severely restrained in the gas-rich models in this phase. It either had vanished or even become negative. The underlying physical process has been quantified by Berentzen et al. (1998): the *gas affects the orbital structure* of the collisionless components, which in turn modifies the bar properties. However, detailed understanding of how this influences particular parameters of the bars requires more work.

We have attempted to clarify this dependence of the bar strength on f_g and ϵ_{grav}. As a working hypothesis, we have tested whether the final mass of the CMC, M_{CMC}, in each model can serve as an underlying hidden parameter replacing f_g and ϵ_{grav}. The dependency of the final bar strength on the CMC mass in the pure stellar disks has been analyzed by Athanassoula et al. (2005). Extensive study of the bar evolution in the presence of an analytical CMC has been performed by Shen & Sellwood (2004). Bournaud et al. (2005) have attributed the bar weakening to both the CMC and the angular momentum transfer from the gas to the stellar bar, using analytical CMC and DM halo. However, the latter process has been found to be unimportant by Berentzen et al. (2007) following a detailed analysis of the angular momentum transfer in live potentials of the CMC and DM halo. Moreover, Berentzen et al. (1998, 2007) have used self-consistently growing CMCs in the gaseous/stellar disks to demonstrate that the secular bar growth is strongly affected. The set of numerical models analyzed here is in fact the most controlled experiment performed so far to test the influence of gas fraction and its resolution on the bar evolution.

Figure 10(a) shows the dependence of the bar strengthening after the first buckling, ΔA_{2b} on final M_{CMC}, with all other parameters characterizing the stellar disk and the DM halo being fixed. One model, SD_G8S1, has been omitted, as its CMC secular evolution is unusually flat and falls out of the sequence with $\epsilon_{grav} = 0.016$. If M_{CMC} is the single defining variable which controls ΔA_{2b}, all three ϵ_{grav}-sequences are expected to merge into a single sequence in Figure 10(a). What is actually observed is that the three sequences exhibit a very similar behavior—each curve is flat for the gas-poor models, experiences an abrupt drop, and flattens out. However, the curves do not coincide completely as would be expected if M_{CMC} were the *unique* underlying parameter. In fact, in some cases the points corresponding to the same M_{CMC} but different ϵ_{grav} have a substantial vertical dispersion in ΔA_{2b}. Hence, the issue remains inconclusive. In contrast, we show the final M_{CMC} value normalized by the disk mass at $t = 0$ as a function of f_g (Figure 10(b)). This fractional M_{CMC} value is indeed unique for the three sequences, as all three curves have nearly merged.

We now turn to a plausible correlation between the buckling amplitude and the bar strengthening. The vertical buckling (e.g., Toomre 1966; Combes et al. 1990; Raha et al. 1991) is a recurrent instability (Martinez-Valpuesta et al. 2006) that was

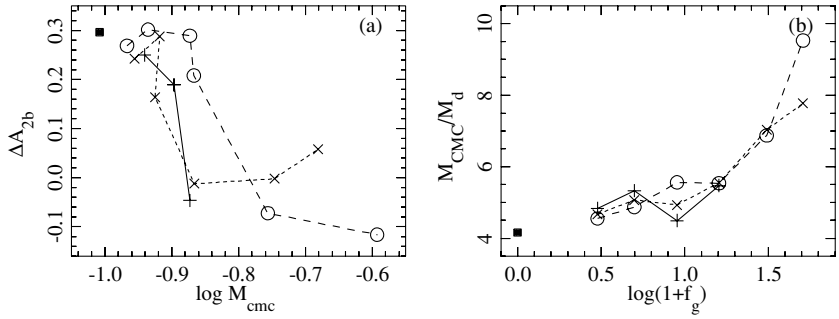

Figure 10. (a) Secular strengthening of the bar, ΔA_{2b}, after the first buckling and until the end of the simulations, as a function of the final central mass concentration (CMC) within $R = 0.1$, M_{CMC}, for different spatial resolution in the gas, abbreviated as in Figure 9. The filled square represents the SD model (Paper I) with no gas. The model SD_G8S1 has been omitted (see the text). (b) Final M_{CMC} normalized by the total mass of the disk at $t = 0$ as a function of f_g.

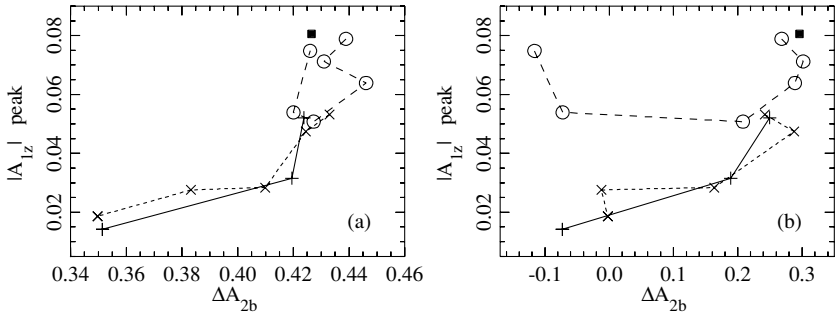

Figure 11. First vertical buckling amplitude of the stellar bar, $A_{1,z}$, as a function of the bar strengthening during dynamical and secular phases of its evolution, ΔA_{2b}, for different spatial resolution in the gas, abbreviated as in Figure 9. The filled square represents the SD model with no gas.

recently analyzed by Berentzen et al. (2007) in the presence of gas (see also Berentzen et al. 1998). The gas component, it has been concluded, leads to a milder instability. Here, we have attempted to relate the buckling amplitude, $A_{1,z}$, to the change in the bar amplitude, ΔA_{2b}, in the dynamical and secular phases of evolution (Figure 11). In both phases, we observe a clear correlation between $A_{1,z}$ and ΔA_{2b}. Stronger bar instability leads to a stronger buckling, and indeed, increasing f_g makes the bar and buckling instabilities milder (Figures 11(a); see also Figure 9(a)). On the other hand, stronger buckling goes in tandem with the bar secular growth (Figure 11(b)). This trend shows saturation for the strongest bars. Higher resolution sequences with $\epsilon_{grav} = 0.016$ and 0.5 behave in a very similar fashion, while the lowest resolution sequence stands out of this correlation. We have also checked the value of the drop in A_{2b} during the buckling and find a clear match between the higher resolution sequences, while the lower resolution models behave differently.

The physical extent of the bar depends on its ability to capture additional orbits. While in principle this capture can proceed at all radii, the fertile region lies between the bar's end and its CR radius, where various families of orbits can be easily destabilized. Therefore, the bar growth due to the orbit capture, should go in tandem with the angular momentum *influx* because the near-CR orbits will have a larger momentum-to-energy, J/E, ratio than the bar orbits. In Paper I, we have shown, and this is confirmed here, that the influx of angular momentum across the CR and into the bar is able to maintain $J_{d,in}$∼const. in time, as long the CR radius lies within the disk, but in the presence of the gas *this statement is limited to the gas-poor models only*. This happens despite that the CR remains within the disk at all times and for all gas-rich models (Figure 4). In other words, in gas-rich models the J influx across the CR cannot compensate for its loss within the CR.

The amplitude A_{2b} is expected to be related to the ability of the bar to capture additional orbits in the bar CR region, leading to its geometrical growth. In both the dynamical and secular phases of the bar evolution we find that the final bar amplitude, A_{2b}, correlates with the final bar size[4] (Figure 12). So stronger bars appear to be longer as well. Taken at face value, this property of bar evolution appears to be supported by recent observations in that the K-band images of barred galaxies exhibit a correlation between the bar amplitude, measured by the $m = 2$ Fourier component, and its size (Elmegreen et al. 2007). However, there are caveats.

We find that the bar sizes are substantially smaller in the gas-rich models compared to the gas-poor ones (Figures 3 and 13). While the median bar size at the end of the simulation in the latter models appears to be ∼1.2, it is around 0.5 in the former ones, i.e., 12 kpc versus 5 kpc, embedded in the identical disks and halos. This difference arises almost entirely during the secular phase of the bar evolution. More precisely, by the end of the dynamical stage, one can notice that the bar size slightly anti-correlates with f_g for the gas-rich models and only for $\epsilon_{grav} = 0.016$ and 0.05 sequences. This trend is sufficiently weak and bars differ by not more than 10%–15% of their length. So essentially, the bar growth in the dynamical phase is independent of f_g.

What is rather striking is the abrupt change in the bar's growth "habit" in the secular phase—bars grow in the gas-poor models and stagnate in the gas-rich ones. This leads to a *bimodal* evolution of the final bar sizes with respect to the gas mass fraction (Figure 13). We note that this diverging evolution should be observable only in the long-lived bars which naturally reside in the older disks. The relevant evolutionary timescale is

[4] The only exception appears to be the low resolution sequence in the dynamical stage whose points cluster in the same region (Figure 12(a)).

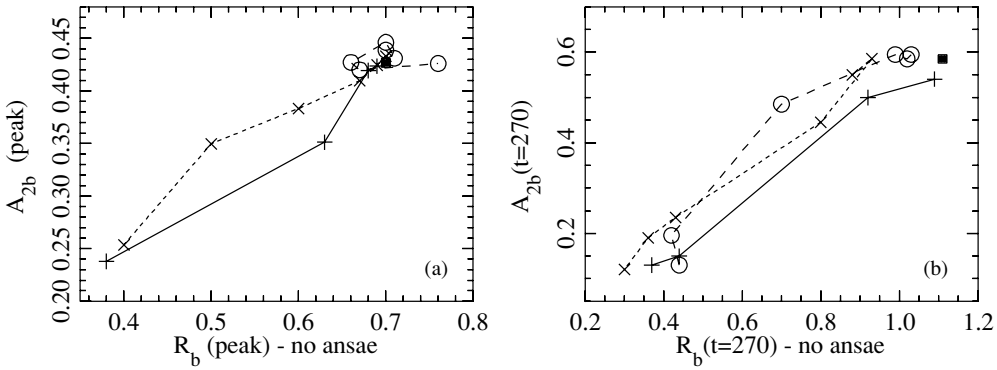

Figure 12. Bar amplitude, A_{2b}, at its pre-buckling peak (left) and at the end of the simulation (right) as a function of the bar size (radius), taken at the same time, during dynamical and secular phases of the bar evolution. Different spatial resolution in the gas has been abbreviated as in Figure 9. The full square represents the SD model with no gas. We have subtracted the *ansae* from the bar sizes given in Figure 3 (more details in the text).

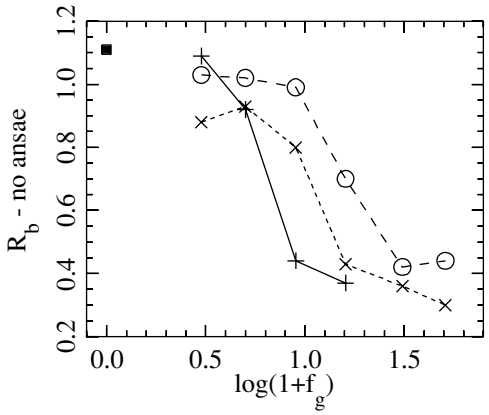

Figure 13. Bimodal distribution of the final bar sizes, $R_b(t = 270)$, as a function of the gas fraction, f_g. We have subtracted the *ansae* from the bar sizes given in Figure 3 (more details in the text).

that of a few Gyr. The Milky Way disk is a good candidate, as it is probably about 10 Gyr old and was not affected by major mergers over this time period (e.g., Gilmore et al. 2002).

The anti-correlation between the final bar sizes and disk gas fractions, found here, complicates the simplistic picture of bar evolution. The reason for this is that our gas-rich models lead to more massive CMCs which increase bulge-to-disk mass ratios and, therefore, should be associated with earlier type disks. This means that smaller bars in our models lie in early-type disks (Figure 13), while they are expected to be found in late-type disks, as noted by a number of surveys (e.g., Erwin 2005; see also Laine et al. 2002). The simplest resolution of this discrepancy can lie in the omission of star formation processes and especially the feedback from stellar evolution and from the central SBHs in this work. This leads to a gross overestimate of the amount of gas which reaches the central kpc and hence contributes to the growth of the CMC by dragging stars and even DM inward. We note, however, that the purpose of this numerical exercise was to understand the effect of gas fraction and gas spatial resolution on the disk–bar–halo interactions in the system. Therefore, we have simplified the long list of processes known to affect the galaxy evolution at large.

In summary, we find that the spatial resolution in the gas component becomes increasingly important for the bar evolution in the gas-rich disks. This is true for the dynamical but especially for the secular phase of evolution. In most cases, model sequences with $\epsilon_{grav} = 0.016$ and 0.05 show a similar behavior, while differing substantially from the sequence with $\epsilon_{grav} = 0.1$.

A bimodal behavior has been found for models based on their gas fractions. The border line between the gas-poor and gas-rich systems appears to lie around 5%–7% for higher resolution models. It shifts to ∼10%–12% for the lowest resolution models. The switch from a gas-poor to a gas-rich behavior appears to be sufficiently abrupt. It is clearly visible in all basic characteristics of bar evolution, such as the bar strength, the CMC mass, the bar buckling amplitude, the bar size, etc. The largest differences in the evolution have been found in the secular phase.

We find that the presence of the gas component severely limits the bar growth and affects its pattern speed evolution. While pure stellar models (Paper I) exhibit a rapid slowdown of the bar tumbling, as known for a long time (e.g., Debattista & Sellwood 1998; Athanassoula 2003), the addition of a substantial amount of gas reverses this trend completely. Furthermore, the CR-to-disk size ratio, R_{cr}/R_d, was determined to be an important dynamic discriminator between various phases of barred disk evolution. Here, we find that the gas-rich models are characterized by $R_{cr}/R_d < 1$ and by $\Omega_b \sim$ const. In these models, Ω_b can even slightly increase with time. In addition, the gas-rich models maintain $R_{cr}/R_b < 2$ which is much more in agreement with observations of stellar bars being fast rotators.

The angular momentum evolution displays the same degree of bimodality with the gas fraction. For low f_g, the total disk J drops steeply and monotonically with time after the buckling, while it decreases weakly for the gas-rich models. The reason for this behavior is of course that the bar amplitude is substantially lower in the gas-rich models. Our attempt to explain this difference between the gas-poor and gas-rich models in terms of the more massive CMCs in the latter ones has been rather inconclusive. We shall return to this issue in the forthcoming work.

Next, we have confirmed our previous claim (Paper I) that the angular momentum, $J_{d,in}$, within the CR radius is maintained at a constant level due to the influx of angular momentum across the CR as it expands. We have extended this statement to the gas-poor models. For the gas-rich models, $J_{d,in}$ drops abruptly to a lower level and stays constant thereafter.

A number of corollaries follow from the above results. We find that the bar strength inversely correlates with the gas fraction, both in the dynamical and secular phases of bar evolution. The only exception seems to be the lowest resolution sequence in the dynamical phase which fails to capture this trend. We also find that the buckling amplitude becomes larger for stronger bars prior to the onset of buckling. On the other hand, the secular growth is most prominent in bars which show a large

buckling amplitude. Finally, we show that stronger bars are also the longest ones throughout both evolutionary phases and that bar sizes anti-correlate with the gas fraction.

We are grateful to our colleagues for numerous discussions. This research has been partially supported by NASA/LTSA/ATP/KSGC and the NSF grants to I.S. C.H. acknowledges the NSF grant.

REFERENCES

Athanassoula, E. 2002, ApJ, 569, L83
Athanassoula, E. 2003, MNRAS, 341, 1179
Athanassoula, E., Lambert, J. C., & Dehnen, W. 2005, MNRAS, 363, 496
Begelman, M. C., & Shlosman, I. 2009, ApJ, 702, L5
Berentzen, I., Heller, C. H., & Shlosman, I. 1998, MNRAS, 300, 49
Berentzen, I., Shlosman, I., Martinez-Valpuesta, I., & Heller, C. H. 2007, ApJ, 666, 189
Bournaud, F., & Combes, F. 2002, A&A, 392, 83
Bournaud, F., Combes, F., & Semelin, B. 2005, MNRAS, 364, L18
Buta, R., Alpert, A. J., Cobb, M. L., Crocker, D. A., & Purcell, G. B. 1998, AJ, 116, 1142
Combes, F., Debbasch, F., Friedli, D., & Pfenniger, D. 1990, A&A, 233, 82
Curir, A., Mazzei, P., & Murante, G. 2007, A&A, 467, 509
Debattista, V. P., & Sellwood, J. A. 1998, ApJ, 493, L5
Dehnen, W. 2002, J. Comput. Phys., 179, 27
Dubinski, J., Berentzen, I., & Shlosman, I. 2009, ApJ, 697, 293
Elmegreen, B. G., Elmegreen, D. M., Knapen, J. H., Buta, R. J., Block, D. L., & Puerari, I. 2007, ApJ, 670, L97
Englmaier, P., & Shlosman, I. 2004, ApJ, 617, L115
Erwin, P. 2005, MNRAS, 364, 283
Friedli, D., & Benz, W. 1993, A&A, 268, 65
Friedli, D., & Martinet, L. 1993, A&A, 277, 27
Gilmore, G., Wyse, R. F. G., & Norris, J. E. 2002, ApJ, 574, L39
Heller, C. H., & Shlosman, I. 1994, ApJ, 424, 84
Heller, C. H., Shlosman, I., & Athanassoula, E. 2007, ApJ, 671, 226
Hernquist, L. 1993, ApJ, 356, 359
Hopkins, P. F., & Quataert, E. 2010, MNRAS, submitted (arXiv:0912.3257)
Knapen, J. H., Beckman, J. E., Heller, C. H., Shlosman, I., & de Jong, R. S. 1995, ApJ, 454, 623
Laine, S., Shlosman, I., Knapen, J. H., & Peletier, R. F. 2002, ApJ, 567, 97
Lynden-Bell, D., & Kalnajs, A. J. 1972, MNRAS, 157, L1
Martinez-Valpuesta, I., Knapen, J. H., & Buta, R. 2007, AJ, 134, 1863
Martinez-Valpuesta, I., & Shlosman, I. 2004, ApJ, 613, L29
Martinez-Valpuesta, I., Shlosman, I., & Heller, C. H. 2006, ApJ, 637, 214
Mundell, C. G., & Shone, D. L. 1999, MNRAS, 304, 475
Pfenniger, D., & Norman, C. A. 1990, ApJ, 363, 391
Raha, N., Sellwood, J. A., James, R. A., & Kahn, F. D. 1991, Nature, 352, 411
Romano-Diaz, E., Shlosman, I., Heller, C. H., & Hoffman, Y. 2009, ApJ, 702, 1250
Sandage, A. 1961, The Hubble Atlas of Galaxies (Washington, DC: Carnegie Inst.)
Sellwood, J. A. 1981, A&A, 89, 296
Shen, J., & Sellwood, J. A. 2004, ApJ, 604, 614
Shlosman, I., Begelman, M. C., & Frank, J. 1990, Nature, 345, 679
Shlosman, I., Frank, J., & Begelman, M. C. 1989, Nature, 338, 45
Shlosman, I., & Noguchi, M. 1993, ApJ, 414, 474
Shlosman, I. 1999, in ASP Conf. Ser. 187, Evolution of Galaxies on Cosmological Timescales, ed. J. E. Beckman & T. J. Mahoney (San Francisco, CA: ASP), 100
Toomre, A. 1966, in Notes on the 1966 Summer Study Program in Geophysical Fluid Dynamics at the Woods Hole Oceanographic Institution, ed. W. V. R. Malkus (Woods Hole, MA: Woods Hole Oceanographic Inst.), 11
Villa-Vargas, J., Shlosman, I., & Heller, C. H. 2009, ApJ, 707, 218 (Paper I)